

Article

Effect of UV-LED Wavelength on Reactive Species Photogeneration from Dissolved Organic Matter

Ze-Chong Guo ^{1,2,3}, Lu Zhang ³, Yong Chen ^{1,*}, Cheng Huang ^{1,2,3} and Zhi-Min Liao ²

¹ School of Environmental and Engineering, Huazhong University of Science and Technology, Wuhan 430074, China; guozechong@just.edu.cn (Z.-C.G.)

² Jiangxi Jindalai Environmental Protection Co., Ltd., Nanchang 330100, China

³ School of Environmental and Chemical Engineering, Jiangsu University of Science and Technology, Zhenjiang 212100, China

* Correspondence: ychen@mail.hust.edu.cn

Abstract: The photogeneration of reactive species from dissolved organic matter (DOM) plays a crucial role in the photochemical and photobiochemical processes in natural aquatic systems. However, the impact of the ultraviolet (UV) wavelength on the photogeneration of reactive species by different sources of DOM remains unclear. In this study, UV light at four wavelengths (365 nm, 310 nm, 280 nm, and 260 nm) provided by UV-LEDs were irradiated onto three types of DOM: humic acid (HA), fulvic acid (FA), and effluent organic matter (EfOM). Three reactive species produced by DOM, including excited triplet-state DOM (³DOM*), singlet oxygen (¹O₂), and hydroxyl radicals (•OH), were determined. UV₃₆₅ proved to be the most efficient wavelength for generating ¹O₂ and •OH, with formation rates of $3.47 \times 10^{-6} \text{ M s}^{-1}$ and $1.67 \times 10^{-8} \text{ M s}^{-1}$, respectively, with the addition of FA and EfOM. The highest steady-state concentrations of all three reactive species were also generated under UV₃₆₅, reaching $3.00 \times 10^{-13} \text{ M}$ (³DOM*) and $1.64 \times 10^{-11} \text{ M}$ (¹O₂) with the FA addition, and $1.44 \times 10^{-10} \text{ M}$ (•OH) with the EfOM. Across the different DOM sources, UV₃₆₅ obtained the maximum quantum yields of reactive species, indicating the stronger effect of UV₃₆₅ on inducing the photosensitization of DOM compared to the other shorter wavelengths. This study expands our understanding of the photochemistry of DOM in aquatic environments.

Keywords: dissolved organic matter; quantum yield; reactive species; steady-state concentration; UV-LED irradiation



Citation: Guo, Z.-C.; Zhang, L.; Chen, Y.; Huang, C.; Liao, Z.-M. Effect of UV-LED Wavelength on Reactive Species Photogeneration from Dissolved Organic Matter. *Water* **2024**, *16*, 635. <https://doi.org/10.3390/w16050635>

Academic Editor: John Zhou

Received: 28 December 2023

Revised: 17 February 2024

Accepted: 19 February 2024

Published: 21 February 2024



Copyright: © 2024 by the authors. Licensee MDPI, Basel, Switzerland. This article is an open access article distributed under the terms and conditions of the Creative Commons Attribution (CC BY) license (<https://creativecommons.org/licenses/by/4.0/>).

1. Introduction

Ultraviolet (UV) radiation has garnered significant attention due to its specific impact on photochemical processes [1,2]. It has been proven to play a key role in remediating contamination in aquatic systems [3]. UV radiation encompasses wavelengths ranging from 100 to 400 nm and is further divided into four bands, namely, UVA (long-wave UV, 320~400 nm), UVB (middle-wave UV, 290~320 nm), UVC (short-wave UV, 200~290 nm), and UVD (vacuum UV, 100~200 nm) [4]. Sunlight serves as the primary source of UV radiation in the environment, with UVA making up approximately 95% of the sunlight radiating to the ground and UVB making up the remaining 5%. Other radiations that are considered harmful to life are largely filtered by the atmosphere [5].

UV irradiation can directly degrade certain classes of contaminants in an aqueous solution, such as iodinated trihalomethanes [6], ametryn [7], fluconazole [8], diclofenac [9], and so on. In addition to direct photodegradation, another significant process in contaminant degradation is the photosensitization that occurs in the presence of dissolved organic matter (DOM). DOM is prevalent in natural aquatic environments and has strong absorption for the sunlight spectrum. When exposed to light irradiation, DOM is excited to the singlet state (¹DOM*) from the ground state (S₀), and the non-steady-state species are prone to transformation through two pathways: (i) the release of energy via fluorescence emissions

and a radiationless transition back to the S_0 , and (ii) by undergoing intersystem crossings through spin–orbital couplings to the excited triplet state ($^3\text{DOM}^*$) [10,11]. $^3\text{DOM}^*$ can directly participate in contaminant remediation through energy or electron-transfer interactions and induce the formation of singlet oxygen ($^1\text{O}_2$) and hydroxyl radicals ($\bullet\text{OH}$) in the presence of oxygen [12]. $\bullet\text{OH}$ are well known for their high efficacy in attenuating a broad range of contaminants, while $^1\text{O}_2$ has also been confirmed to enhance the degradation of certain contaminants and pathogenic microorganisms [13]. For instance, the photodegradation of 17 α -ethinylestradiol was notably enhanced by the addition of DOM, with the contributions of direct and photosensitization degradation identified as 27% and 73%, respectively [14]. The degradation of roxithromycin was also confirmed to be promoted by DOM, with the photogeneration of hydroxyl radicals ($\bullet\text{OH}$) identified as the major contributor to the photosensitization effect [15]. Understanding the photoreactivity of DOM is essential for assessing the fate of organic contaminants in aquatic systems.

The photochemical behaviors of different types of DOM are known to be closely correlated with their source and molecular characteristics [16]. Natural DOM, primarily originating from allochthonous sources, is composed of humic acid (HA) and fulvic acid (FA), with an apparent molecular weight ranging from 1.5 to 7 kDa. With the increasing capacity of wastewater treatment, the discharge of effluent into the natural environment is on the rise. In some waterways, effluent from wastewater treatment has become the dominant component, which emphasizes the importance of understanding the photochemical effects of effluent organic matter (EfOM) [12]. EfOM is primarily autochthonous and mainly comprises soluble microbial products and macromolecules with a higher apparent molecular weight exceeding 20 kDa [17]. In comparison to terrestrial-origin DOM, such as HA and FA, EfOM generally exhibits fewer aromatic constituents, specific UV absorbance at 254 nm, and higher apparent quantum yields of reactive species [18].

The photochemical behaviors of various types of DOM induced by UV irradiation have been extensively reported. However, the impact of the UV wavelength on the efficiency of reactive species photogeneration is still unrevealed. In previous investigations, mercury lamps and xenon lamps were frequently utilized as illumination sources, which normally provide broad emission spectra rather than single-wavelength emission spectra [16]. With the advancement of light-emitting diode (LED) technology, UV-LEDs have emerged as a promising alternative to traditional UV-light sources. They offer advantages such as emissions at a single wavelength, higher energy efficiency, a longer lifespan, more constant light intensity, and improved heating control [19].

In this work, four UV-LED lights with wavelengths of 365 nm (UVA), 310 nm (UVB), 280 nm (UVC), and 260 nm (UVC) were employed to investigate their impacts on the generation of photochemically produced reactive intermediates. The photosensitization effects of three DOM sources, namely, HA, FA, and EfOM, were compared across various UV-LED wavelengths. The steady-state concentrations and quantum yields of the reactive species ($^3\text{DOM}^*$, $^1\text{O}_2$, and $\bullet\text{OH}$) were systematically assessed. The results of this study enhance our understanding of DOM photosensitization and reactive species generation in natural water systems, and they can contribute to the development of UV-LED-based photochemical water treatment technologies.

2. Materials and Methods

2.1. Photochemical Irradiation Experiment

Irradiation experiments were conducted in a customized quartz beaker featuring a diameter of 3.85 cm, an empty volume of 50 mL, and a working volume of 40 mL, as illustrated in Figure 1. The UV-LED light source (Yonglin Optoelectronics Co., Ltd., Shenzhen, China) was affixed to the outside of the bottom of the beaker, as described in previous literature [20]. The photochemical reactor was placed on a magnetic stirrer that provided a stirring speed of 400 rpm to achieve a homogeneous mixture. A hole with a rubber stopper was made in the cover of the quartz lid to facilitate sampling with disposable syringes. In the experimental setup, a DOM solution (5.0 mg C L^{-1}) with a probe molecule

at pH 7.0 was added into the reactor. Then, the solution underwent irradiation using an LED light source, and aliquots of 0.5 mL were periodically withdrawn at predetermined intervals from the reactor for analysis.

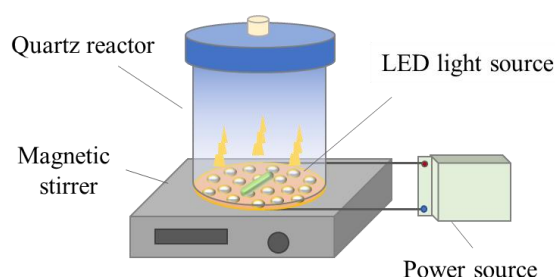


Figure 1. Schematic diagram of reactor configuration.

2.2. Materials

Wastewater effluent (EfOM) was obtained from a local wastewater treatment plant in Wuhan, China. The EfOM sample was isolated by a solid-phase extraction process using PPL cartridges (Agilent Technologies, Santa Clara, CA, USA), as previously reported. Humic acid (HA) and fulvic acid (FA) were purchased from Henan Changsheng Chemical Co., Ltd (Luohe, China) and Sigma-Aldrich (St. Louis, MO, USA), respectively, and they were purified according to the method widely accepted by the International Humic Substances Society (IHSS). All DOM samples were stored in the dark and kept at 4.0 °C before the experiments.

Molecule probes, including 2,4,6-trimethylphenol (TMP) (99%), Furfuryl alcohol (FFA) (99%), and Terephthalic acid (TPA) (99%), were all purchased from Sigma-Aldrich (St. Louis, MO, USA). Mobile phases, including acetonitrile and methanol, were liquid-chromatographic-grade. Others were analytical-reagent-grade. Deionized water was used in all experiments.

2.3. UV-LED Intensity Determination

The intensities of the four UV-LED light sources were determined before the photochemical reaction experiment. The light intensities of the UV-LEDs with wavelengths of 260 nm, 280 nm, and 310 nm were measured using iodide/iodate chemical actinometry [21]. The 365 nm UV-LED intensity was estimated by potassium ferrioxalate actinometry [22]. The light intensities and corresponding irradiances of the UV-LED light sources under different wavelengths are presented in Table 1.

Table 1. Light intensities and irradiances of UV-LEDs under different wavelengths.

Wavelength (nm)	Light Intensity (mW cm ⁻²)	Light Irradiance (Einstein L ⁻¹ s ⁻¹)
260	0.93	5.87×10^{-7}
280	3.16	2.15×10^{-6}
310	5.49	4.14×10^{-6}
365	1.18	1.05×10^{-6}

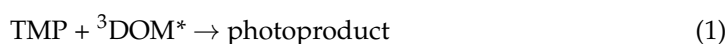
2.4. Detection of Reactive Species

TMP, FFA, and TPA were commissioned as molecular probes for the ³DOM*, ¹O₂, and •OH, respectively. These compounds were chosen because their direct degradation processes were inactive, and their molar absorption coefficients and quantum yields were found to be negligible. The quantification of the TMP, FFA, and photoproduct of TPA (HTPA) was carried out using high-performance liquid chromatography (Essentia LC-15C, Shimadzu, Kyoto, Japan) equipped with a UV-vis detector (Essentia SPD-15C) and an HC-C18 column (5 μm, 250 mm × 4.6 mm, Agilent, USA). TMP was determined at a detection wavelength of 280 nm, utilizing acetonitrile, water, and phosphoric acid (v:v:v = 70:30:0.1)

as the mobile phases with a flow rate of 1.0 mL min⁻¹; FFA was determined at 220 nm with a mobile phase of methanol and water (*v:v* = 35:65) under a flow rate of 1.0 mL min⁻¹; HTPA was detected at 315 nm using acetonitrile and water (*v:v* = 33:67) with a flow rate of 0.8 mL min⁻¹.

In the determination of the ³DOM*, the solutions were sparged with N₂ to eliminate the dissolved oxygen during the entire reaction period. For the measurements of both the ³DOM* and ¹O₂, methanol (0.1 M) was introduced to quench the photogeneration of the •OH. The degradation rate constants of the TMP (*k*_{TMP}) and FFA (*k*_{FFA}), as well as the formation rate constant of the HTPA (*k*_{HTPA}), were obtained by fitting the data based on pseudo-first-order kinetics.

In this study, the value of the formation rate of the ³DOM* (*R*_{3DOM*}) is approximately equal to the initial transformation rate of the TMP (*R*_{TMP}) because the scavenging rate of the TMP was much greater than the physical quenching constant of the ³DOM*. The *R*_{3DOM*} and the steady-state concentration of the ³DOM* can be calculated with the following equations:



$$\frac{d[\text{TMP}]}{dt} = -k_{\text{TMP},{}^3\text{DOM}^*}[\text{TMP}][{}^3\text{DOM}^*]_{\text{ss}} \quad (2)$$

$$R_{3\text{DOM}^*} \approx R_{\text{TMP}} = k_{\text{TMP}}[\text{TMP}]_0 \quad (3)$$

where [³DOM*]_{ss} is the steady-state concentration of the ³DOM*, M; [TMP] is the concentration of TMP, M; [TMP]₀ is the initial concentration of TMP, 500 μM; *k*_{TMP,3DOM*} is the reaction rate constant, 3.0 × 10⁹ M⁻¹ s⁻¹ [23,24].

The steady-state concentration of ¹O₂ and the formation rate of ¹O₂ (*R*_{1O₂}) was quantified by the concentration variation in the FFA according to the following equations:



$$\frac{d[\text{FFA}]}{dt} = -k_{\text{FFA},{}^1\text{O}_2}[\text{FFA}][{}^1\text{O}_2]_{\text{ss}} \quad (5)$$

$$k_{\text{FFA}} = k_{\text{FFA},{}^1\text{O}_2} \frac{R_{1\text{O}_2}}{k_{\text{FFA},{}^1\text{O}_2}[\text{FFA}]_0 + k_{1\text{O}_2}} \quad (6)$$

where [¹O₂]_{ss} is the steady-state concentration of ¹O₂, M; [FFA] is the concentration of FFA, M; [FFA]₀ is the initial concentration of FFA, 50 μM; *k*_{FFA,1O₂} is the reaction rate constant, 8.3 × 10⁷ M⁻¹ s⁻¹ [25,26]; *k*_{1O₂} is the physical quenching rate of ¹O₂, 2.5 × 10⁵ M⁻¹ s⁻¹ [10].

The steady-state concentration of the •OH and the formation rate of the •OH (*R*_{•OH}) were quantified by the detection of the HTPA (fluorescent), which is the single-hydroxylation product of TPA (non-fluorescent) [27], according to the following equations:



$$\frac{d[\text{HTPA}]}{dt} = 0.35 \times k_{\text{TPA},\bullet\text{OH}}[\text{TPA}][\bullet\text{OH}]_{\text{ss}} = 0.35 \times R_{\bullet\text{OH}} \quad (8)$$

where [•OH]_{ss} is the steady-state concentration of •OH, M; [HTPA] and [TPA] are the concentrations of HTPA and TPA, M; *k*_{TPA,•OH} is the reaction rate constant, 3.3 × 10⁹ M⁻¹ s⁻¹ [26,28].

2.5. Quantum Yield Calculation

The quantum yields of the ³DOM*, ¹O₂, and •OH were calculated as follows:

$$\Phi_i = \frac{R_i}{I_0(1 - 10^{\epsilon_{\lambda}bc})} \quad (9)$$

where R_i is the formation rate of the $^3\text{DOM}^*$, $^1\text{O}_2$, and $\bullet\text{OH}$ in the DOM solutions, $\text{M}\cdot\text{s}^{-1}$; I_0 is the incident light intensity obtained by the actinometers, $\text{Einstein L}^{-1} \text{s}^{-1}$; ϵ_λ is the absorption coefficient of the DOM at a specific wavelength, $\text{L mg}^{-1} \text{cm}^{-1}$; b is the path length, cm ; c is the concentration of the DOM, mg L^{-1} .

3. Results and Discussion

3.1. DOM Characteristics

The absorption spectra of the FA, HA, and EfOM utilized in this study exhibited broad and unstructured profiles, displaying an expected near-exponential decrease with the increasing wavelength in the ultraviolet and visible wavelengths (Figure 2). The absorption coefficients of the FA, HA, and EfOM were determined at wavelengths of 260 nm, 280 nm, 310 nm, and 365 nm and are summarized in Table 2. Among the three types of DOM, the FA displayed the highest absorption, followed by the HA, while the EfOM presented the lowest absorption. Based on the absorption spectra, the E2/E3 ratios (the ratio of absorbance at 254 nm and 365 nm), which are believed to be negatively correlated with the humification, aromaticity degree, and molecular weight of the DOM [29], were 2.3, 2.5, and 4.2 for the HA, FA, and EfOM, respectively. The evident differences in the UV–vis absorption spectra among the three DOM samples highlighted significant variations in their structures and compositions, which strongly influence their photochemistry.

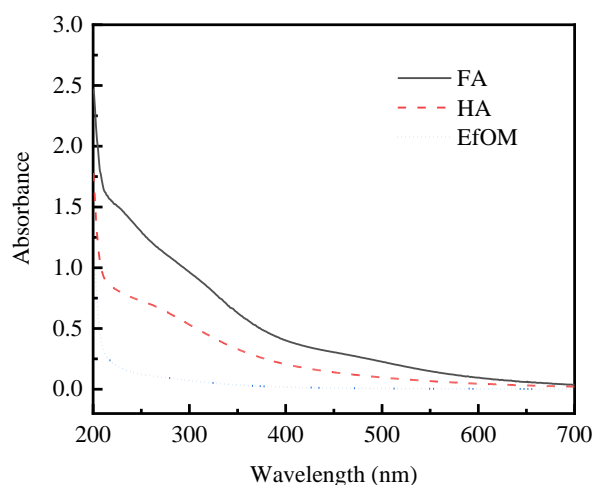


Figure 2. UV–vis absorption spectra of HA, FA, and EfOM ($[\text{DOM}] = 10 \text{ mg C L}^{-1}$, $\text{pH} = 7.0$).

Table 2. Absorption coefficients of DOM samples at different wavelengths.

DOM	Absorption Coefficient (ϵ_λ , $\text{L mg}^{-1} \text{cm}^{-1}$)			
	365 nm	310 nm	280 nm	260 nm
FA	0.0542	0.0902	0.1086	0.1215
HA	0.0285	0.0488	0.0620	0.0698
EfOM	0.0028	0.0063	0.0090	0.0110

3.2. Reactive Species Formation under UV-LED Irradiation

The reactivities of the reactive species with the probe molecules under various wavelengths of UV-LED irradiation are depicted in Figure 3. In the case of the TMP, the molecule probe for the $^3\text{DOM}^*$, a linear degradation pattern was observed, with the slopes of UV-LED₃₆₅ noticeably higher than those of the other irradiation wavelengths when HA and FA were added. UV-LED₂₈₀ demonstrated a comparable effect to UV-LED₃₆₅ in the EfOM group. Concerning the FFA, the molecule probe for the $^1\text{O}_2$, UV-LED₃₆₅ exhibited the highest degradation effect in all the DOM conditions, indicating the most efficient $^1\text{O}_2$ formation compared to the other wavelengths. The rate of HTPA (the molecule probe for

•OH) formation was higher with the HA and FA additions under UV-LED₂₈₀; however, UV-LED₃₆₅ appeared to be more efficient with the EfOM addition.

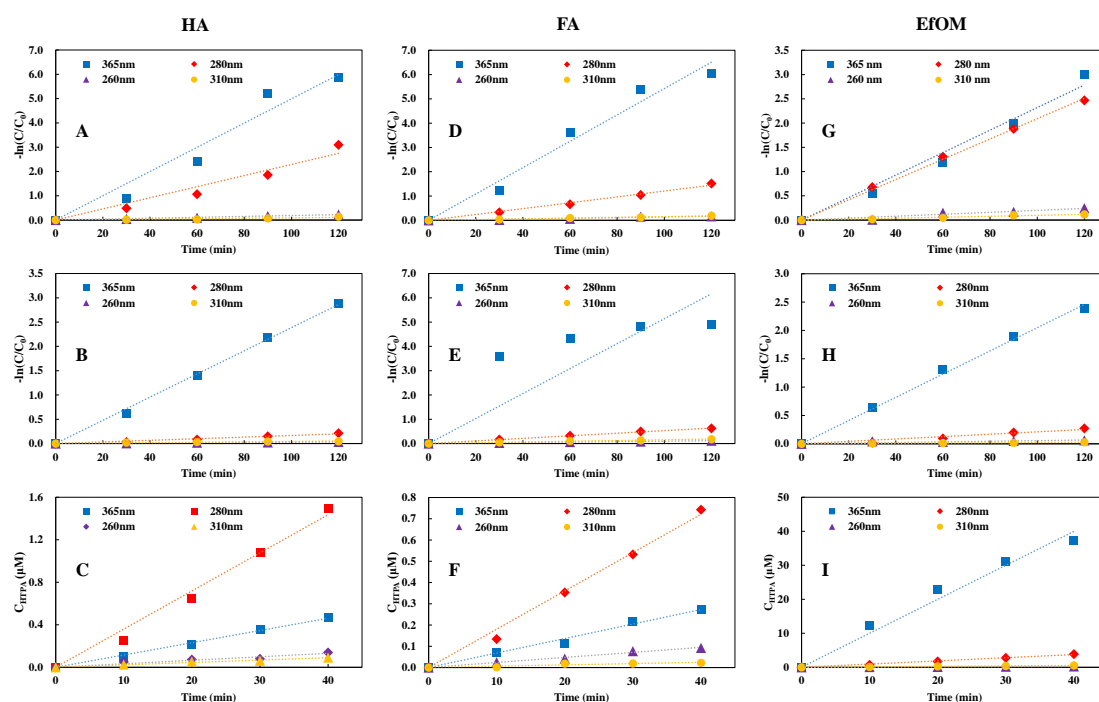


Figure 3. Reactivities of ${}^3\text{DOM}^*$ ((A) ${}^3\text{HA}^*$; (D) ${}^3\text{FA}^*$; (G) ${}^3\text{EfOM}^*$), ${}^1\text{O}_2$ (B,E,H), and $\bullet\text{OH}$ (C,F,I) with probe molecules as a function of time under various wavelengths of UV-LED irradiation. (A,D,G) TMP, 500 μM ; (B,E,H) FFA, 50 μM ; and (C,F,I) TPA, 1 mM ($[\text{DOM}] = 5 \text{ mg C L}^{-1}$, pH = 7.0).

The formation of reactive species was significantly influenced by the variation in the DOM type, as detailed in Table 3. The HA and FA exhibited similar ${}^3\text{DOM}^*$ reaction rates under all irradiation conditions, with the highest k_{TMP} values recorded at 0.0536 and 0.0541 min^{-1} , respectively, under UV-LED₃₆₅. The corresponding formation rates ($R_{3\text{DOM}^*}$) were 4.62×10^{-7} and $4.66 \times 10^{-7} \text{ M s}^{-1}$, respectively. For the EfOM, UV-LED₃₆₅ and UV-LED₂₈₀ provided similar k_{TMP} values of 0.0232 and 0.0209 min^{-1} , with $R_{3\text{DOM}^*}$ values of 2.00×10^{-7} and $1.80 \times 10^{-7} \text{ M s}^{-1}$, respectively.

Table 3. Reaction rate constants (k) for probe molecules and formation rates (R) of reactive species at various UV-LED light wavelengths.

DOM	Wavelength (nm)	k_{TMP} (min^{-1})	k_{FFA} (min^{-1})	k_{HTPA} (min^{-1})	$R_{3\text{DOM}^*}$ (10^{-7} M s^{-1})	$R_{1\text{O}_2}$ (10^{-7} M s^{-1})	$R_{\bullet\text{OH}}$ ($10^{-10} \text{ M s}^{-1}$)
HA	365	0.0536	0.0244	0.0118	4.62	9.52	5.48
	310	0.0011	0.0004	0.0022	0.09	0.17	1.10
	280	0.0252	0.0018	0.0381	2.17	0.77	17.10
	260	0.0019	0.0003	0.0031	0.16	0.13	1.57
FA	365	0.0541	0.0817	0.0068	4.66	34.72	1.10
	310	0.0016	0.0015	0.0006	0.14	0.64	0.10
	280	0.0125	0.0053	0.0180	1.08	2.25	3.00
	260	0.0016	0.0010	0.0024	0.14	0.43	0.40
EfOM	365	0.0232	0.0205	0.9997	2.00	8.71	166.60
	310	0.0010	0.0002	0.0138	0.09	0.09	2.30
	280	0.0209	0.0021	0.0934	1.80	0.89	15.60
	260	0.0020	0.0005	0.0059	0.17	0.21	0.90

The peak reaction rates of the FFA appeared at 365 nm, irrespective of the DOM type, surpassing those at the other wavelengths by at least one order of magnitude. The highest k_{FFA} was 0.0817 min^{-1} by the FA, being 2.3- and 3.0-fold higher than those by the HA and EfOM, respectively. Correspondingly, the maximum formation rate of $^1\text{O}_2$ ($R_{1\text{O}_2}$) was $34.72 \times 10^{-7} \text{ M s}^{-1}$ with the FA addition, and it was considerably lower in the HA and EfOM, recorded at 9.52 and $8.71 \times 10^{-7} \text{ M s}^{-1}$ under UV-LED₃₆₅. The k_{HTPA} in the EfOM group was noticeably higher than in the HA and FA groups, reaching 0.9997 min^{-1} at the wavelength of 365 nm, corresponding to a $\bullet\text{OH}$ ($R_{\bullet\text{OH}}$) formation rate of $166.60 \times 10^{-10} \text{ M s}^{-1}$, two orders of magnitude higher than in the HA and FA. These results indicate that the EfOM, particularly under the irradiation of 365 nm, was much more efficient at $\bullet\text{OH}$ formation.

3.3. Steady-State Concentration of Reactive Species

The steady-state concentration of reactive species is a key parameter for investigating photochemical processes and their environmental impacts. The steady-state concentrations of the $^3\text{DOM}^*$, $^1\text{O}_2$, and $\bullet\text{OH}$ are summarized in Figure 4. $^3\text{DOM}^*$ is an important source of reactive oxygen species and can transform into $^1\text{O}_2$ and $\bullet\text{OH}$ upon UV irradiation. In the group with the HA addition, the steady-state concentrations of the $^3\text{HA}^*$ were $10.6 \times 10^{-15} \text{ M}$, $140.0 \times 10^{-15} \text{ M}$, $6.1 \times 10^{-15} \text{ M}$, and $297.8 \times 10^{-15} \text{ M}$, respectively, under irradiations of 260 nm, 280 nm, 310 nm, and 365 nm UV-LEDs (see Figure 4A). This indicates that UV-LED₂₈₀ and UV-LED₃₆₅ were more efficient at the photosensitization of $^3\text{HA}^*$ generation, with the $[^3\text{HA}^*]_{\text{ss}}$ of UV-LED₃₆₅ being about 1.1-fold higher than that of UV-LED₂₈₀. UV-LED₃₆₅ was beneficial for the photogeneration of $^1\text{O}_2$ and yielded an $[^1\text{O}_2]_{\text{ss}}$ of $4.9 \times 10^{-12} \text{ M}$, which was about 60, 13, and 80 times higher than that under UV-LED₂₆₀, UV-LED₂₈₀, and UV-LED₃₁₀, respectively. In contrast to the $^3\text{HA}^*$ and $^1\text{O}_2$, the peak $[\bullet\text{OH}]_{\text{ss}}$ of $51.8 \times 10^{-17} \text{ M}$ was recorded under UV-LED₂₈₀ irradiation, and it was 2.2-fold higher than that under 365 nm.

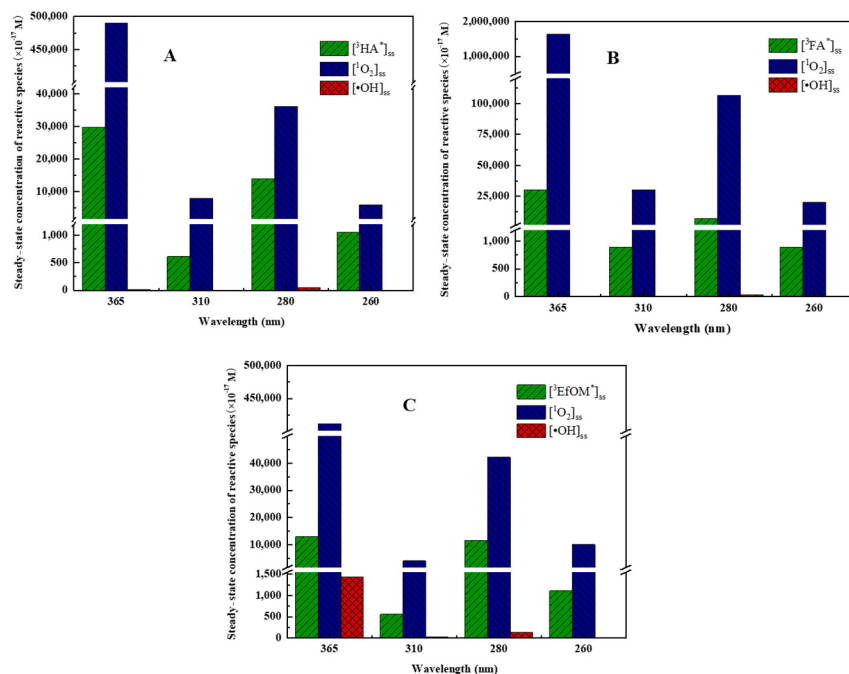


Figure 4. Steady–state concentrations of $^3\text{DOM}^*$, $^1\text{O}_2$, and $\bullet\text{OH}$ at HA (A), FA (B), and EfOM (C), adding conditions at varying wavelengths of 260 nm, 280 nm, 310 nm, and 365 nm.

For the FA, the influences of the UV-LED wavelength on the photogeneration of $^1\text{O}_2$ and $^3\text{FA}^*$ were quite similar (Figure 4B). The maximum $[^3\text{FA}^*]_{\text{ss}}$ of $300.6 \times 10^{-15} \text{ M}$ and $[^1\text{O}_2]_{\text{ss}}$ of $16.41 \times 10^{-12} \text{ M}$ were observed under UV-LED₃₆₅, which were about 2.3-fold

and 15-fold higher those of UV-LED₂₈₀. Irradiations of UV-LED₃₁₀ and UV-LED₂₆₀ were inefficient, with steady-state concentrations two orders of magnitude lower. UV-LED₂₈₀ was the most efficient for •OH generation, demonstrating a [$\bullet\text{OH}$]_{ss} of 26.0×10^{-17} M, followed by UV-LED₃₆₅ (9.8×10^{-17} M) and UV-LED₂₆₀ (3.5×10^{-17} M). The photosensitization for •OH formation was inferior under UV-LED₃₁₀ irradiation.

In the experiment with the EfOM addition (Figure 4C), UV-LED₃₆₅ appears to be the most efficient for reactive species generation compared to UV-LED₃₁₀, UV-LED₂₈₀, and UV-LED₂₆₀. The highest steady-state concentrations of [$^3\text{EfOM}^*$]_{ss}, [$^1\text{O}_2$]_{ss}, and [$\bullet\text{OH}$]_{ss} were 128.9×10^{-15} M, 41.2×10^{-13} M, and 1.4×10^{-14} M, respectively. UV-LED₂₈₀ exhibited a similar performance in $^3\text{EfOM}^*$ photogeneration to that of UV-LED₃₆₅, with a [$^3\text{EfOM}^*$]_{ss} of 116.1×10^{-15} M. Similarly, the photosensitizations of UV-LED₃₁₀ and UV-LED₂₆₀ were relatively weak, and the production of reactive species was remarkably low.

Among all the reactive species, $^1\text{O}_2$ emerged as the predominant species under various wavelength conditions, with the [$^1\text{O}_2$]_{ss} consistently surpassing both the $^3\text{DOM}^*$ and [$\bullet\text{OH}$]_{ss}, fluctuating within a wide range. Typically, the steady-state concentration of $^1\text{O}_2$ in natural aquatic environments is reported to be from around 10^{-15} to 10^{-13} M L⁻¹ [30]. However, in this study, the maximum [$^1\text{O}_2$]_{ss} reached 4.1×10^{-10} M L⁻¹ in the presence of the FA addition under UV₃₆₅, indicating a substantial formation of $^1\text{O}_2$ through the photosensitization of FA induced by UV₃₆₅. In addition to $^1\text{O}_2$, •OH also play a critical role in the degradation of pollutants and other processes in natural waters. As previous reported, the steady-state concentration of •OH in natural water is typically from around 10^{-18} to 10^{-16} M L⁻¹ [31]. The maximum [$\bullet\text{OH}$]_{ss} in this study obtained with the addition of EfOM under UV₃₆₅ was notably higher, reaching a value of 3.6×10^{-13} M L⁻¹. With such a considerable level of •OH, the system with the EfOM addition under UV₃₆₅ would be highly beneficial for the removal of organic pollutants.

In general, the steady-state concentrations of the $^3\text{DOM}^*$, $^1\text{O}_2$, and •OH were remarkably influenced by the types of DOM. Higher [$^3\text{DOM}^*$]_{ss} values were obtained in the HA and FA addition groups, and the [$^1\text{O}_2$]_{ss} was most pronounced in the presence of FA, while EfOM was found to be most beneficial for •OH generation. The UV-LED wavelengths exhibited a consistent impact on the varying trends of the reactive species concentrations across all the DOM addition conditions. Among these, UV-LED₃₆₅ demonstrated the most pronounced benefits for reactive species generation, followed by UV-LED₂₈₀, which was generally from one to two orders of magnitude higher than those observed under UV-LED₃₁₀ and UV-LED₂₆₀.

3.4. Quantum Yields

Quantum yields of reactive species serve as crucial indicators to unveil the formation efficiency and dynamics of reactive species, offering a comprehensive insight into the photochemical behaviors of different types of DOM. The quantum yields were estimated using the reactive species formation rates (refer to Table 3), irradiation intensities (see Table 1), and absorption coefficients (see Table 2), as shown in Table 4.

Table 4. Quantum yields of $^3\text{DOM}^*$, $^1\text{O}_2$, and •OH at various UV-LED wavelengths ([DOM] = 5 mg C L⁻¹, pH = 7.0).

Wavelength (nm)	HA			FA			EfOM		
	$\Phi_{^3\text{HA}^*}$ ($\times 10^{-2}$)	$\Phi_{^1\text{O}_2}$ ($\times 10^{-2}$)	$\Phi_{\bullet\text{OH}}$ ($\times 10^{-4}$)	$\Phi_{^3\text{FA}^*}$ ($\times 10^{-2}$)	$\Phi_{^1\text{O}_2}$ ($\times 10^{-2}$)	$\Phi_{\bullet\text{OH}}$ ($\times 10^{-4}$)	$\Phi_{^3\text{EfOM}^*}$ ($\times 10^{-2}$)	$\Phi_{^1\text{O}_2}$ ($\times 10^{-2}$)	$\Phi_{\bullet\text{OH}}$ ($\times 10^{-4}$)
365	65.2	134.5	7.7	50.4	375.5	1.2	180.0	785.2	1501.4
310	0.3	0.5	0.3	0.3	1.6	0.02	0.9	0.9	2.5
280	11.0	3.9	8.7	5.1	10.6	1.4	27.8	13.8	24.1
260	2.9	2.3	2.8	2.4	7.3	0.7	8.3	10.2	4.3

The quantum yields of reactive species were significantly influenced by the DOM types. Specifically, the EfOM exhibited higher quantum yields than the other DOM samples across various reactive species. It was efficient in $^3\text{DOM}^*$ formation, with the $\Phi_{^3\text{DOM}^*}$ 2.5–5.5 times higher compared to those of the HA and FA. The trends closely mirrored those of the $\Phi_{^3\text{DOM}^*}$, and the $\Phi_{^1\text{O}_2}$ of the EfOM surpassed those of the HA and FA, except under UV₃₁₀. Notably, the $\Phi_{\bullet\text{OH}}$ of the EfOM exceeded those of the other DOM samples, with a maximum increase of 1251 times (compared to FA under 365 nm).

Previous reports have indicated higher triplet-state photo quantum yields for EfOM than the reference natural organic matter [32]. Another study observed higher quantum yields of $^3\text{DOM}^*$, $^1\text{O}_2$, and $\bullet\text{OH}$ formation under simulated sunlight irradiation for EfOM compared to HA and FA [10], which is consistent with this study's findings. According to prior literature [16,33], the quantum yield of reactive species is positively correlated with the E2/E3 of the DOM. The higher E2/E3 ratio of EfOM (4.2) compared with those of HA (2.3) and FA (2.5) explains its outstanding performance in reactive species production.

In addition to DOM, the wavelength notably impacts the quantum yield of each reactive species. UV-LED₃₆₅ exhibited the maximum $\Phi_{^3\text{DOM}^*}$ across all the DOM samples, being 5.9–9.8 times higher than that of UV-LED₂₈₀, and remarkably higher than those under 260 nm and 310 nm. This indicates that the DOM samples effectively absorbed incident photons and were excited to $^3\text{DOM}^*$ under 365 nm UV irradiation. The $\Phi_{^1\text{O}_2}$ for all the DOM samples exhibited consistent patterns under different wavelengths, with 34.5–56.8 times higher values than UV-LED₂₈₀, and two orders of magnitude higher values than the other wavelengths. DOM is a major source of $\bullet\text{OH}$ in natural water systems, and $\bullet\text{OH}$ generation is related to the $^3\text{DOM}^*$ oxidation process. In this study, the $\Phi_{\bullet\text{OH}}$ was two orders of magnitude lower than the $\Phi_{^3\text{DOM}^*}$ and $\Phi_{^1\text{O}_2}$. With the addition of HA and FA, the $\Phi_{\bullet\text{OH}}$ was similar under 365 nm and 280 nm irradiation and obviously higher than at 310 nm and 260 nm. In the EfOM addition group, UV-LED₃₆₅ substantially enhanced the $\Phi_{\bullet\text{OH}}$, being 62 times that under 280 nm. Given $\bullet\text{OH}$'s strong oxidizability, the high-level photosensitization of EfOM at UV-LED₃₆₅ will be favorable for the photodegradation of organic contaminants.

The quantum yields of reactive species are influenced by both the formation rates and light intensities. With higher formation rates and a relatively low light intensity (slightly higher than 310 nm but lower than 260 nm and 280 nm), UV₃₆₅ achieved the maximum quantum yields of all the reactive species across the different sources of DOM. This suggests that UV-LED₃₆₅ is more effective at inducing the photosensitization of DOM compared to other shorter wavelengths in the UVB and UVC bands. In water photocatalytic treatment using UV-LEDs, UVC light is typically chosen and believed to facilitate photocatalytic degradation more easily due to its higher energy. However, the results of this study present an alternative perspective. Specifically, the findings of the efficient generation of $^1\text{O}_2$ and $\bullet\text{OH}$ under UV₃₆₅ with the EfOM addition provides a new technical option based on UV-LED for treating micro-polluted water containing EfOM.

4. Conclusions

In the current study, the impact of the UV-LED wavelength on the reactive species formation from various types of DOM was investigated. The different DOM samples exhibited diverse preferences in reactive species generation: FA was found to be beneficial for the $^1\text{O}_2$ and $^3\text{DOM}^*$ formation, while EfOM facilitated the $\bullet\text{OH}$ generation. Among all the wavelengths, UV₃₆₅ displayed the highest steady-state concentrations of reactive species, with 3.00×10^{-13} M [$^3\text{DOM}^*$]_{ss} and 1.64×10^{-11} M [$^1\text{O}_2$]_{ss} by the FA addition, and 1.44×10^{-10} M [$\bullet\text{OH}$]_{ss} by the EfOM. Moreover, the quantum yields of UV₃₆₅ for all the reactive species were remarkably higher than those of the other wavelengths across all the DOM samples. This result not only broadens our understanding of the photochemistry of DOM in natural water systems, but it also provides guidance for the development of UV-LED-based water treatment technology.

Author Contributions: Z.-C.G.: investigation and writing—original draft. L.Z.: data processing. Y.C.: conceptualization and supervision. C.H.: funding, review, and editing. Z.-M.L.: writing—review and editing. All authors have read and agreed to the published version of the manuscript.

Funding: This research was funded by the National Natural Science Foundation of China, No. 52000090, the Natural Science Foundation of Jiangsu Province, No. BK20201001, and the China Postdoctoral Science Foundation, No. 2021M701511.

Data Availability Statement: Data are contained within the article.

Conflicts of Interest: Authors Ze-Chong Guo, Cheng Huang, Zhi-Min Liao were employed by the company Jiangxi Jindalai Environmental Protection Co., Ltd. The remaining authors declare that the research was conducted in the absence of any commercial or financial relationships that could be construed as a potential conflict of interest.

References

1. Qian, L.; Georgi, A.; Gonzalez-Olmos, R.; Kopinke, F.-D. Degradation of perfluorooctanoic acid adsorbed on Fe-zeolites with molecular oxygen as oxidant under UV-A irradiation. *Appl. Catal. B Environ.* **2020**, *278*, 119283. [[CrossRef](#)]
2. Silva, M.P.; Lastre-Acosta, A.M.; Mostafa, S.; McKay, G.; Linden, K.G.; Rosario-Ortiz, F.L.; Teixeira, A.C.S.C. Photochemical generation of reactive intermediates from urban-waste bio-organic substances under UV and solar irradiation. *Environ. Sci. Pollut. Res. Int.* **2017**, *24*, 18470–18478. [[CrossRef](#)] [[PubMed](#)]
3. Chen, J.; Loeb, S.; Kim, J.H. LED revolution: Fundamentals and prospects for UV disinfection applications. *Environ. Sci. Water Res. Technol.* **2017**, *3*, 188–202. [[CrossRef](#)]
4. Hockberger, P.E. A History of Ultraviolet Photobiology for Humans, Animals and Microorganisms. *Photochem. Photobiol.* **2002**, *76*, 561–579. [[CrossRef](#)]
5. Widel, M.; Krzywon, A.; Gajda, K.; Skonieczna, M.; Rzeszowska-Wolny, J. Induction of bystander effects by UVA, UVB, and UVC radiation in human fibroblasts and the implication of reactive oxygen species. *Free Radic. Biol. Med.* **2014**, *68*, 278–287. [[CrossRef](#)]
6. Xiao, Y.; Fan, R.; Zhang, L.; Yue, J.; Webster, R.D.; Lim, T.-T. Photodegradation of iodinated trihalomethanes in aqueous solution by UV 254 irradiation. *Water Res.* **2014**, *49*, 275–285. [[CrossRef](#)] [[PubMed](#)]
7. Martins de Oliveira, D.; Pereira Cavalcante, R.; de Melo da Silva, L.; Sans Mazón, C.; Esplugas Vidal, S.; Oliveira, S.C.D.; Machulek, A., Jr. Identification of intermediates, acute toxicity removal, and kinetics investigation to the Ametryn treatment by direct photolysis (UV254), UV254/H₂O₂, Fenton, and photo-Fenton processes. *Environ. Sci. Pollut. Res. Int.* **2019**, *26*, 4348–4366. [[CrossRef](#)] [[PubMed](#)]
8. Chen, Z.-F.; Ying, G.-G.; Jiang, Y.-X.; Yang, B.; Lai, H.-J.; Liu, Y.-S.; Pan, C.-G.; Peng, F.-Q. Photodegradation of the azole fungicide fluconazole in aqueous solution under UV-254: Kinetics, mechanistic investigations and toxicity evaluation. *Water Res.* **2014**, *52*, 83–91. [[CrossRef](#)]
9. Kim, I.; Tanaka, H. Photodegradation characteristics of PPCPs in water with UV treatment. *Environ. Int.* **2009**, *35*, 793–802. [[CrossRef](#)]
10. Wan, D.; Sharma, V.K.; Liu, L.; Zuo, Y.; Chen, Y. Mechanistic Insight into the Effect of Metal Ions on Photogeneration of Reactive Species from Dissolved Organic Matter. *Environ. Sci. Technol.* **2019**, *53*, 5778–5786. [[CrossRef](#)]
11. McNeill, K.; Canonica, S. Triplet state dissolved organic matter in aquatic photochemistry: Reaction mechanisms, substrate scope, and photophysical properties. *Environ. Sci. Process. Impacts* **2016**, *18*, 1381–1399. [[CrossRef](#)]
12. O'Connor, M.; Helal, S.R.; Latch, D.E.; Arnold, W.A. Quantifying photo-production of triplet excited states and singlet oxygen from effluent organic matter. *Water Res.* **2019**, *156*, 23–33. [[CrossRef](#)]
13. Mostafa, S.; Rosario-Ortiz, F.L. Singlet oxygen formation from wastewater organic matter. *Environ. Sci. Technol.* **2013**, *47*, 8179–8186. [[CrossRef](#)]
14. Ren, D.; Huang, B.; Bi, T.; Xiong, D.; Pan, X. Effects of pH and dissolved oxygen on the photodegradation of 17 α -ethynylestradiol in dissolved humic acid solution. *Environ. Sci. Process. Impacts* **2016**, *18*, 78–86. [[CrossRef](#)]
15. Lv, B.L.; Li, W.; Yu, X.L.; Zhang, D.; Zhang, Y.L. Effect of dissolved organic matter on the photodegradation of roxithromycin. *Acta Sci. Circumstantiae* **2019**, *39*, 747–754.
16. Cai, T.; Zhang, X.; Zhang, S.; Ming, Y.; Zhang, Q. Photochemical behaviors of dissolved organic matter in aquatic environment: Generation, characterization, influencing factors and practical application. *Environ. Res.* **2023**, *231*, 116174. [[CrossRef](#)] [[PubMed](#)]
17. Cai, M.-H.; Wu, Y.-P.; Ji, W.-X.; Han, Y.-Z.; Li, Y.; Wu, J.-C.; Shuang, C.-D.; Korshin, G.V.; Li, A.-M.; Li, W.-T. Characterizing property and treatability of dissolved effluent organic matter using size exclusion chromatography with an array of absorbance, fluorescence, organic nitrogen and organic carbon detectors. *Chemosphere* **2020**, *243*, 125321. [[CrossRef](#)] [[PubMed](#)]
18. Wan, D.; Kong, Y.; Wang, X.; Selvin Simpson, S.; Sharma, V.K.; Zuo, Y.; Chen, Y. Effect of permanganate oxidation on the photoreactivity of dissolved organic matter for photodegradation of typical pharmaceuticals. *Sci. Total Environ.* **2022**, *813*, 152647. [[CrossRef](#)] [[PubMed](#)]
19. Muramoto, Y.; Kimura, M.; Nouda, S. Development and future of ultraviolet light-emitting diodes: UV-LED will replace the UV lamp. *Semicond. Sci. Technol.* **2014**, *29*, 084004. [[CrossRef](#)]

20. Wan, D.; Yang, J.; Wang, X.; Xiang, W.; Selvinsimpson, S.; Chen, Y. Wavelength-Dependent Photoreactivity of Root Exudates from Aquatic Plants under UV-LED Irradiation. *ACS EST Water* **2022**, *2*, 2613–2622. [[CrossRef](#)]
21. Wang, W.-L.; Wu, Q.-Y.; Li, Z.-M.; Lu, Y.; Du, Y.; Wang, T.; Huang, N.; Hu, H.-Y. Light-emitting diodes as an emerging UV source for UV/chlorine oxidation: Carbamazepine degradation and toxicity changes. *Chem. Eng. J.* **2016**, *310*, 148–156. [[CrossRef](#)]
22. Hatchard, C.G.; Parker, C.A.; Bowen, E.J. A new sensitive chemical actinometer—II. Potassium ferrioxalate as a standard chemical actinometer. *Proc. R. Soc. Lond. Ser. A Math. Phys. Sci.* **1956**, *235*, 518–536.
23. McCabe, A.J.; Arnold, W.A. Reactivity of triplet excited states of dissolved natural organic matter in stormflow from mixed-use watersheds. *Environ. Sci. Technol.* **2017**, *51*, 9718–9728. [[CrossRef](#)] [[PubMed](#)]
24. Halladja, S.; ter Halle, A.; Aguer, J.-P.; Boulkamh, A.; Richard, C. Inhibition of Humic Substances Mediated Photooxygenation of Furfuryl Alcohol by 2,4,6-Trimethylphenol. Evidence for Reactivity of the Phenol with Humic Triplet Excited States. *Environ. Sci. Technol.* **2007**, *41*, 6066–6073. [[CrossRef](#)] [[PubMed](#)]
25. Latch, D.E.; Stender, B.L.; Packer, J.L.; Arnold, W.A.; McNeill, K. Photochemical Fate of Pharmaceuticals in the Environment: Cimetidine and Ranitidine. *Environ. Sci. Technol.* **2003**, *37*, 3342–3350. [[CrossRef](#)] [[PubMed](#)]
26. Zhang, D.; Yan, S.; Song, W. Photochemically induced formation of reactive oxygen species (ROS) from effluent organic matter. *Environ. Sci. Technol.* **2014**, *48*, 12645–12653. [[CrossRef](#)] [[PubMed](#)]
27. Page, S.E.; Arnold, W.A.; McNeill, K. Terephthalate as a probe for photochemically generated hydroxyl radical. *J. Environ. Monit.* **2010**, *12*, 1658–1665. [[CrossRef](#)] [[PubMed](#)]
28. Mark, G.; Tauber, A.; Laupert, R.; Schuchmann, H.-P.; Schulz, D.; Mues, A.; von Sonntag, C. OH-radical formation by ultrasound in aqueous solution—Part II: Terephthalate and Fricke dosimetry and the influence of various conditions on the sonolytic yield. *Ultrason. Sonochem.* **1998**, *5*, 41–52. [[CrossRef](#)] [[PubMed](#)]
29. Dalrymple, R.M.; Carfagno, A.K.; Sharpless, C.M. Correlations between Dissolved Organic Matter Optical Properties and Quantum Yields of Singlet Oxygen and Hydrogen Peroxide. *Environ. Sci. Technol.* **2010**, *44*, 5824–5829. [[CrossRef](#)] [[PubMed](#)]
30. Ossola, R.; Jönsson, O.M.; Moor, K.; McNeill, K. Singlet Oxygen Quantum Yields in Environmental Waters. *Chem. Rev.* **2021**, *121*, 4100–4146. [[CrossRef](#)]
31. Vione, D.; Minella, M.; Maurino, V.; Minero, C. Indirect Photochemistry in Sunlit Surface Waters: Photoinduced Production of Reactive Transient Species. *Chem. Eur. J.* **2014**, *20*, 10590–10606. [[CrossRef](#)] [[PubMed](#)]
32. Zhou, H.; Yan, S.; Lian, L.; Song, W. Triplet-State Photochemistry of Dissolved Organic Matter: Triplet-State Energy Distribution and Surface Electric Charge Conditions. *Environ. Sci. Technol.* **2019**, *53*, 2482–2490. [[CrossRef](#)] [[PubMed](#)]
33. Zhou, H.; Lian, L.; Yan, S.; Song, W. Insights into the photo-induced formation of reactive intermediates from effluent organic matter: The role of chemical constituents. *Water Res.* **2017**, *112*, 120–128. [[CrossRef](#)] [[PubMed](#)]

Disclaimer/Publisher’s Note: The statements, opinions and data contained in all publications are solely those of the individual author(s) and contributor(s) and not of MDPI and/or the editor(s). MDPI and/or the editor(s) disclaim responsibility for any injury to people or property resulting from any ideas, methods, instructions or products referred to in the content.